



## PAPER

View Article Online  
View Journal | View Issue

Cite this: *Biomater. Sci.*, 2023, **11**, 2750

# Multifunctional zwitterionic microneedle dressings for accelerated healing of chronic infected wounds in diabetic rat models†

Yuqing Cai,<sup>‡</sup> Xiaodong Xu,<sup>‡</sup> Minmin Wu, Jiaqi Liu, Jie Feng \* and Jing Zhang \*

Diabetic infected wounds are one of the major threats to public health but traditional wound dressings always have poor therapeutic efficacy influenced by the single treatment principle and limited penetration depth. Herein, we developed a novel kind of multifunctional degradable and removable zwitterionic microneedle dressings that could achieve multi-effective treatment of diabetic chronic wounds with a single dressing application. The substrates of microneedle dressings are composed of zwitterionic polymer polysulfobetaine methacrylate (PSBMA) and photothermal hair particles (HMPs), which can absorb wound exudate, form a barrier to the bacterial environment for the wound and exhibit an excellent photothermal bactericidal effect to promote wound healing. By loading zinc oxide nanoparticles (ZnO NPs) and asiaticoside in needle tips, drugs could diffuse in the wound area as the tips degrade to achieve highly effective antibacterial and anti-inflammatory effects and promote deep wound healing and tissue regeneration. The microneedles (MNs) were applied in diabetic rats with *Staphylococcus aureus*-infected wounds to demonstrate that the combination of drug and photothermal multi-treatment has accelerated tissue regeneration and collagen deposition and significantly promoted wound healing.

Received 20th December 2022,  
Accepted 18th February 2023

DOI: 10.1039/d2bm02101c

rsc.li/biomaterials-science

## Introduction

Chronic wounds are one of the great threats to public health, especially the healing of chronic infected wounds in diabetic patients.<sup>1,2</sup> The poor glycemic control in diabetic patients leads to a reduction in the mobility of leukocytes and their role in the removal of pathogenic microorganisms, resulting in rapid bacterial growth in wounds that is difficult to control. In addition, the migration of bacteria and fungi from the skin surface to the subcutaneous tissue through the epidermis and dermis, and the low utilization of antimicrobial drugs lead to an inefficient treatment of wound inflammation and slow the wound healing.<sup>3</sup> Traditional wound dressings can hardly address this type of problem.<sup>4</sup> Therefore, there is an urgent need to develop an effective and novel practical protocol.

Wound healing is usually divided into three main stages: inflammation, tissue formation, and tissue reconstruction.<sup>5</sup> Thus, the development of a multifunction platform that makes

wounds free from inflammation and also promotes cell proliferation and tissue reconstruction has become critical. As known, infection always happens in chronic infected wounds because bacterial biofilms are usually formed to hinder the penetration of drugs and weaken therapy outcomes. Thus, the first thing is to find an effective drug delivery method to resolve this issue.

Microneedle patches are devices capable of transdermal drug delivery across the skin barrier, thus allowing drug access to the cutaneous microcirculation and systemic drug delivery,<sup>6</sup> enhancing the efficacy of the drug. Recently, transdermal drug delivery by microneedles has become one of the most promising drug delivery modalities,<sup>7</sup> due to their advantages such as painlessness, safety, sustainable drug delivery, and ease of handling.<sup>8,9</sup> Hence, microneedle patches are very useful to be applied on chronic infected wounds to achieve highly effective antibacterial and anti-inflammatory effects and promote deep wound healing and tissue regeneration.

Most polymeric materials commonly used for wound dressings can be made into microneedle patches, including natural polymers such as maltose, alginate, gelatin, cellulose, and hyaluronic acid, as well as some synthetic polymers.<sup>10</sup> Among these materials, zwitterionic materials have emerged as robust candidates for wound dressings because they show excellent antifouling properties that can initially resist the adhesion of bacteria.<sup>11–13</sup> However, their applications in microneedle patches have been rarely explored to date. Thus, we

College of Materials Science and Engineering, Zhejiang University of Technology, Hangzhou, Zhejiang, 310014, P. R. China. E-mail: zhangjing@zjut.edu.cn, fengjie@zjut.edu.cn

†Electronic supplementary information (ESI) available: The degradation of M MNs. Morphological changes of microneedles before and after pressure. Body weight change curve of SD rats. Blood glucose value of SD rats before and after treatment. See DOI: <https://doi.org/10.1039/d2bm02101c>

‡These authors contributed to this work equally.

were eager to prepare zwitterionic microneedle patches for chronic wound healing. However, resisting the external bacterial adhesion is not enough to inhibit the growth of bacteria already existing in the wound area. Therefore, anti-bacterial agents should be introduced into the zwitterionic microneedles.

According to literature, about 76% of the bacteria isolated from diabetic wounds are *Staphylococcus aureus*,<sup>14</sup> and severely infected wounds may have enhanced drug resistance due to misuse of antibiotics, which may even threaten patients' lives.<sup>15</sup> To meet drug delivery requirements to minimize antibiotic concentrations and control bacterial resistance, many strategies have been explored instead of antibiotics. In previous studies, it has been proved that near-infrared light-induced photothermal therapy (PTT) can effectively kill bacteria and accelerate wound healing. So, the incorporation of photothermal agents into zwitterionic microneedle substrates will obtain antifouling and antibacterial wound dressings without worry about drug resistance. Many photothermal agents, including inorganic materials (black phosphorus, CuS, etc.) and organic materials (protein-based materials, etc.) have been developed for PTT.<sup>16,17</sup> Hair is composed mainly of melanin and keratin, two polymers that are ideal for biomedical applications. Compared with other photothermal agents, HMPs extracted from hair have the advantages of low cost, high conversion rate, low immunogenicity, and biocompatibility.<sup>18,19</sup> Thus, HMPs are very suitable for the construction of photothermal wound dressings.

As mentioned above, besides anti-infection, deep wound healing and tissue regeneration are also important for chronic wound healing in diabetes. It is well documented that some metal ions (e.g.,  $Mg^{2+}$ ,  $Zn^{2+}$ , and  $Cu^{2+}$ ) as trace elements required by the human body, are not only useful to inhibit bacterial infections and bypass antibiotic resistance, but also can aid in cell proliferation and tissue regeneration.<sup>12,20</sup> Therefore, these metal ions have become more favorable for application in wound healing compared to traditional antibiotics. Taking the advantages of microneedles, the metal ions loaded in the tips of the microneedles can be delivered to the deep layer of the wound to kill the interior bacteria and promote tissue regeneration.

Here, we developed a kind of zwitterionic microneedle patch for diabetic infected wounds with multiple therapeutic effects. The zwitterionic hydrogel substrates can be used as a hydrogel dressing to resist external bacterial adhesion and absorb wound exudate to maintain a suitable moist environment conducive to better wound recovery.<sup>21</sup> The prepared HMPs were loaded into the microneedle substrates as photothermal converters to provide excellent photothermal properties to achieve more efficient bactericidal effects.

Also, by loading ZnO NPs and asiaticoside into the degradable zwitterionic tips of the microneedle, a drug release effect in the dermis is achieved. ZnO NPs have excellent antibacterial and anti-inflammatory properties that promote acute and chronic wound healing, inhibit bacterial growth at the wound site, and can resist some existing bacterial resistance.<sup>22–26</sup> Asiaticoside, the main component obtained by isolation and purification of *Centella asiatica*, has been shown to have a

good promotion effect in diabetic chronic wound healing.<sup>18</sup> Benefiting from ZnO NPs and asiaticoside, the killing of bacteria deep in the wound and promotion of tissue healing at the wound site would be realized, thus achieving a multifunctional, high-efficiency, and low-cost therapeutic platform effect.

## Materials and methods

### Materials

[2-(Methacryloyloxy)ethyl] dimethyl-(3-sulfopropyl) (SBMA), chitosan (viscosity: 45 mPa s), ammonium persulfate (APS), and methacrylic anhydride were purchased from Aladdin. HRP-IgG protease, Roswell Park Memorial Institute (RPMI) 1640 medium, fetal bovine serum (FBS), and sterile phosphate-buffered saline (PBS) were purchased from Invitrogen Corp. Other reagents and solvents in the experiment were provided by Shanghai Reagent Chemical Co. (China). All reagents in this research were used as received without purification.

### Preparation of degradable crosslinking agent

According to the method in the literature,<sup>27</sup> 5 g of chitosan (CS) was dissolved in 100 ml of 5 wt% deionized water acetic acid solution and then stirred at 60 °C for 30 min. After 10 mL of methacrylic anhydride was added to the solution at 50 °C, the reaction was continued at 50 °C for 4 h. Finally, the crude product was dialyzed at 25 °C for three days and lyophilized.

### Synthesis of ZnO NPs

3.72 mM of zinc acetate dihydrate was dispersed in 20 mL of anhydrous ethanol, and then condensed and refluxed at 68 °C for 90 min. After that, 8.22 mM of potassium hydroxide (KOH) was dissolved in 10 mL of anhydrous ethanol. The above KOH ethanol solution was added dropwise to the cooled zinc acetate ethanol solution, and reacted at room temperature for 1 h. Then, 1 mL of (3-aminopropyl)triethoxysilane (APTES) was added to the above solution, and reacted at room temperature for 2 h. Finally, the ZnO NPs were obtained by centrifugation and washing with deionized water<sup>28</sup>

### Synthesis of HMPs

HMPs were prepared by the alkali extraction method. Firstly, 2 g of hair was heated in 1 M NaOH solution and dissolved under magnetic stirring for 1 h. Then, the dissolved hair particles in NaOH solution were dialyzed in deionized water for 2 days. Next, the solution was centrifuged at 2000 rpm for 6 min to remove large particles, and then centrifuged at 12 000 rpm for 10 min to obtain HMPs. Finally, the HMPs were lyophilized and used after several washes.

### Fabrication of the degradable microneedle system

**Preparation of the microneedle tips.** Firstly, 10 mg of APS and 6 mg of CS-MA were added to 1 mL of 3 M SBMA solution to make a microneedle prepolymer solution, and then 1 mg of ZnO NPs and 8 mg of asiaticoside were added to this prepolymer solution and stirred well. Finally, the above solutions were

added to the microneedle molds and evacuated, and then dried after the excess solution was removed.

**Formation of the microneedle substrates.** 3 M SBMA was dissolved in deionized water, and then 1 mg mL<sup>-1</sup> HMPs, 1 mg mL<sup>-1</sup> *N,N'*-methylene-bis-acrylamide (MBA) and 10 mg mL<sup>-1</sup> APS were added to the solution successively and stirred until the solution was uniform. This homogeneous mixture is added to the mold in which the tips are prepared. After drying for 2–4 h, the intact microneedles were carefully peeled from the mold.

### Characterization of the nanoparticles and the microneedles (MNs)

**Characterization of nanoparticles.** The morphology of nanoparticles was observed by transmission electron microscopy (TEM; Tecnai F30).

**Characterization of MNs.** The morphology of the prepared MNs was observed using a scanning electron microscope (SEM; Hitachi S-4700) and an equipped digital microscope (Instron 5966, USA). The mechanical property of the MNs was tested on a universal testing machine at room temperature (RT) in air. For the compression test, the prepared MNs were placed on a chassis and then compressed at a compression rate of 2 mm min<sup>-1</sup>.

**Degradation of the tips of the MNs.** The entire tips were soaked in PBS, and the tip degradation process was observed, photographed, and recorded.

### Light-activated thermal properties of MNs *in vitro*

To investigate whether the microneedle substrates have photo-thermal properties and to determine the optimal loading concentration of HMPs, the temperature change profiles of the substrates were measured (808 nm, 1–2 W cm<sup>-2</sup>, 3 min) with 0, 0.5 and 1 mg mL<sup>-1</sup> HMP concentration. Thermal images and the real-time temperature of the substrates were acquired and detected using a professional thermal imager (UTi120S).

To evaluate the photothermal stability and reproducibility of the microneedle substrates, the substrates were irradiated with NIR light (808 nm, 1.5 W cm<sup>-2</sup>) for 5 on/off cycles. In each cycle, the microneedle substrate was exposed to NIR light for 3 min, and then the NIR light was turned off until the temperature dropped to room temperature. During this process, the temperature change of the substrates was recorded using an infrared thermographic camera.

### Swelling behavior and water retention of microneedle substrates

**Microneedle substrates swelling.** In brief, microneedle substrates of the same size (13.5 cm × 13.5 cm) were weighed ( $W_d$ ) and then immersed in simulated wound exudate (AWE) at 37 °C. AWE was prepared by dissolving DMEM in PBS with pH = 6.2 and adding 10% (v/v) pig serum.<sup>29</sup> After a pre-determined period, the swollen substrates were taken out and weighed again ( $W_t$ ).

The Swelling ratio is obtained from the following equation:

$$\text{Swelling ratio} = \frac{W_t - W_d}{W_t}$$

**Water retention of the substrates.** The swollen microneedle substrates were weighed ( $W_s$ ) and placed at 37 °C. The weight of the substrates ( $W_t$ ) was weighed at predetermined periods and recorded until the dry weight ( $W_d$ ) was restored.

The water retention rate is obtained from the following equation:

$$\text{Water retention rate} = \frac{W_t - W_d}{W_s - W_d}$$

### Anti-protein adhesion test

The swollen and sterilized MNs were added to a 24-well plate, and 1 mL of HRP-conjugated goat anti-human IgG (IgG/HRP) solution at a concentration of 1 mL mL<sup>-1</sup> was added into each well. Then, the plate was incubated in a thermostat at 37 °C for 12 h. After that, the MNs were immersed in PBS for 0.5 h and 3 h, respectively. After 0.5 h, the first group was removed, rinsed several times in PBS, and placed in a new 24-well plate. After 3 h, the other group was removed, rinsed several times, and put into a new 24-well plate. Then, a freshly prepared citrate phosphate buffer (pH = 5) solution containing *o*-phenylenediamine (1 mg mL<sup>-1</sup>) and hydrogen peroxide (0.03 vol%) was added to each well, and the reaction was suspended with sulfuric acid (2 M in equal volume) after 15 min. Finally, the optical density (OD) of the supernatant was measured at 492 nm by a microplate reader. The above steps were repeated five times.

### *In vitro* antibacterial activity

*Staphylococcus aureus* and *Escherichia coli* were used as model bacteria to study the *in vitro* antibacterial activity of MNs. First, the prepared MNs were added to 12-well plates and co-cultured with bacteria in Luria-Bertani (LB) medium at a concentration of 1 × 10<sup>6</sup> CFU mL<sup>-1</sup>. Then, the 24-well plates were exposed to near-infrared light at 808 nm (1.5 W cm<sup>-2</sup>) for 10 min. After irradiation, 30 μL of bacterial solution from each well was diluted with 10 mL PBS. Then, 50 μL of the diluted bacteria solution was applied to the solid medium, and further incubated in an incubator for 14 h. The experiment was divided into four groups ( $n = 3$ ):

Control: Only the bacterial solution was applied as a control group.

Blank MNs: Blank microneedles without NIR irradiation.

HMP MNs + NIR: Microneedles-loading HMPs in the substrates with NIR irradiation.

M MNs: Microneedles-loading ZnO NPs and asiaticoside in the tips without NIR irradiation.

M-HMP MNs + NIR: Microneedles-loading ZnO NPs and asiaticoside in the tips and HMPs in the substrates with NIR irradiation.

### Biocompatibility analysis

**Application of MNs to skin *ex vivo*.** After the pig skin was pretreated at 37 °C for 30 min, the MNs were inserted into the pig skin with the appropriate force for 30 s. After removing the MNs from the pig skin, the holes were dyed with red dye.

Subsequently, the holes were photographed and recorded every 30 s until the hole marks disappeared.

**In vitro cytotoxicity.** 200 mg MNs samples were incubated in 2 mL of RPMI 1640 medium containing 10% fetal bovine serum (FBS) and 1% penicillin–streptomycin double-antibody solution at 37 °C for 24 h. The concentration of MNs sample leaching solution obtained was recorded as 100 mg mL<sup>-1</sup>. Mouse fibroblast (L929) cells at a density of 5 × 10<sup>3</sup> cells per well were inoculated in 96-well plates under standard cell culture conditions (5% CO<sub>2</sub>, 37 °C) for 24 h. After that, the culture solution was removed, and microneedle leaching solutions of different concentrations were added separately. Then, the cells were incubated for another 24 h. Subsequently, all culture solutions were removed, and 200 mL of fresh culture solution and 20 mL of a homogeneous mixture of 5 mg mL<sup>-1</sup> MTT solution were added. After incubation for 4 h, all solutions were carefully removed and 200 mL DMSO was added to each well. The plates were shaken for 15 min, and the absorbance (OD) at 492 nm was measured by a fluorescence microplate reader (DG5033A).

The formula for calculating the relative cell viability is:

$$\text{Relative cell viability} = \frac{\text{OD}_{\text{treated}} - \text{OD}_{\text{blank}}}{\text{OD}_{\text{control}} - \text{OD}_{\text{blank}}} \times 100\%$$

Where the OD<sub>treated</sub>, OD<sub>control</sub>, and OD<sub>blank</sub> are the absorbance of sample wells with MNs leachate, control wells with fresh culture solution, and empty wells, respectively. The OD values were measured based on five independent parallel samples, and the results were expressed as the mean ± standard deviation (SD).

### In vivo wound healing experiments

All animal experiments described herein were in accordance with the requirements of the Animal Ethics Committee of Zhejiang Center of Laboratory Animals, China (ZJCLA-IACUC-20020092). Diabetic infection wound model establishment: after overnight fasting, diabetic rats were made by tail vein injection of streptozotocin (STZ) prepared in citrate buffer (0.1 M, pH 4.5) (50 mg kg<sup>-1</sup>, i.p.). After the STZ injection, the blood glucose level of all rats was measured daily with a blood glucose meter for half a month. Fifteen days later, circular wounds with a diameter of 1 cm were made in rats with elevated blood glucose (more than 11.1 mM). Subsequently, 100 mL of *Staphylococcus aureus* bacterial suspension was applied to the wound site, and the wounds were kept horizontal after the placement of bacterial fluid to establish a diabetic infection wound model. After 24 h of bacterial deposition, the wounds were observed.

**Wound treatment:** model rats were treated with saline treatment (Control), commercially available hydrogel wound dressing (Duoderm), M MNs, HMP MNs, and M-HMP MNs. Finally, all experimental rats were separated and provided with adequate water and food, and the required treatment samples were changed daily. The wound area was observed and photographed on days 0, 1, 3, 5, 7 and 10 to record the wound recovery situation (*n* = 4). On the 10th day, the rats were euthanized.

The tissue samples were fixed with paraformaldehyde (Beyotime, 4% (w/v)) immediately after removal from the rat back for subsequent examination (hematoxylin and eosin (H&E) and Masson's trichrome staining (MTC)). Granulation tissue is the red “robust” tissue that appears during the wound-healing phase and consists of fibroblasts, inflammatory cells, and new blood vessels. Based on these characteristics, the granulation tissue was divided and quantified, and the thickness of each group was obtained. Stained sections were observed and photographed with inverted fluorescence microscopy and a stereomicroscope. Finally, quantitative analysis of granulation tissue and collagen deposits in the stained section photographs was performed using Image J software.

### Statistical analysis

All the data were expressed as the mean or mean ± standard deviations (SD). The statistical analysis was performed with a Student's *t*-test. If the *p*-value is lower than 0.05, the difference is considered significant.

## Results and discussion

As shown in Fig. 1, the multifunctional zwitterionic microneedle dressing is composed of degradable tips to deliver drugs to the deep wound and a hydrogel substrate as a wound dressing. ZnO NPs and asiaticoside were loaded in the tips and HMPs were loaded in the substrate. They were expected to work together to accelerate the healing of the chronically infected wound in the diabetic rat models.

Herein, ZnO NPs were made according to our previous study.<sup>28</sup> As shown in Fig. 2a, the TEM image confirmed the uniform particle size of ZnO NPs, which were about 3 nm in diameter. HMPs were extracted from hair according to the existing method<sup>18</sup> and observed by TEM (Fig. 2b). The obtained HMPs were found to be short rod-shaped, about 800 nm long and 200 nm wide. In a typical experiment, M-HMP MNs were fabricated by a vacuum drying method on a

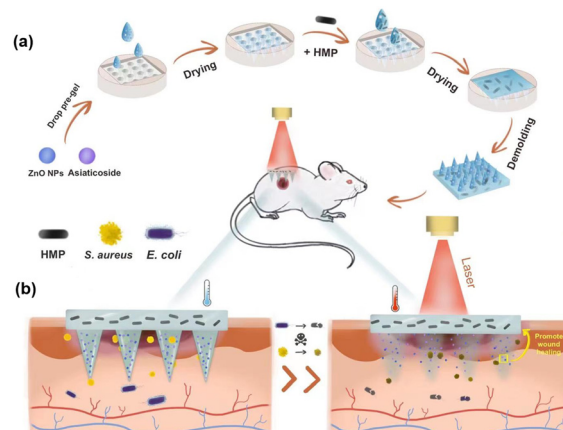


**Fig. 1** Schematic illustration of (a) the preparation of M-HMP MNs and (b) M-HMP MNs for wound healing.



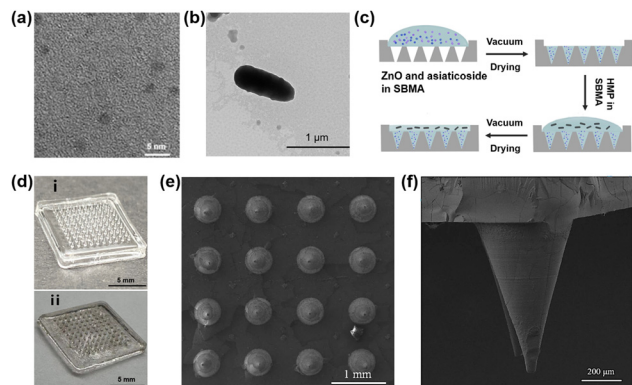


**Fig. 2** (a) TEM image of ZnO NPs. (b) TEM image of individual HMPs. (c) Schematic illustration of the preparation process of the M-HMP MNs. (d) Digital image of the (i) Blank MNs and (ii) M-HMP MNs. (e) SEM image of the MNs. (f) SEM image of amplified tips.

$13.5 \times 13.5 \text{ mm}^2$  substrate having a  $10 \times 10$  array of tips (Fig. 2c). Fig. 2d is the digital image of the MNs. As shown in the SEM image (Fig. 2e), the MNs tips are conical in shape with a base diameter of 390 nm, a distance of 1000 nm between the centers of the two needles, and a height of 1000 nm (Fig. 2f). Since the tips of MNs were made by chitosan-crosslinked PSBMA, they could degrade in PBS within 30 min (Fig. S1†) and gradually release the loaded drugs in the deep wound.

According to the literature, ZnO NPs with a few nanometers in diameter show fluorescence under UV light irradiation and have a bactericidal effect.<sup>28</sup> The results (Fig. 3a and b) showed that the tips of M-HMP MNs with the added ZnO NPs have obvious fluorescence under UV light irradiation, while there is no fluorescence in the blank microneedles. This indicated that the ZnO NPs were successfully loaded in the M-HMP MNs tips. To demonstrate the photothermal effect of M-HMP MNs, the temperature changes of the microneedles were tested under the irradiation of 808 nm NIR light, and the microneedles without HMPs were set as the control. Fig. 4a and b show that the M-HMP MNs warmed up rapidly and exceeded 50 °C within 180 s. Conversely, the microneedles without HMPs had no photothermal effect under NIR light irradiation. The different phenomena further proved that the HMPs had been successfully loaded in the substrates, and the photothermal effect was owing to the loaded HMPs.

Next, to confirm whether the mechanical strength of the prepared MNs could be inserted into the skin, microneedles were prepared using different SBMA concentrations and their displacement-force curves were investigated (Fig. 3c). MNs made from SBMA with a monomer concentration of 3 M has better mechanical strength than those made from 2 M SBMA. The microneedle loadings with ZnO NPs and asiaticoside were subjected to a force of about 2.7 N per needle with a displacement of 0.5 mm, suggesting that they had sufficient strength to penetrate the skin surface (Fig. 3d).<sup>30</sup> In addition to this, the tips of the microneedles were only bent but not broken after the compression test (Fig. S2†), which further proved that

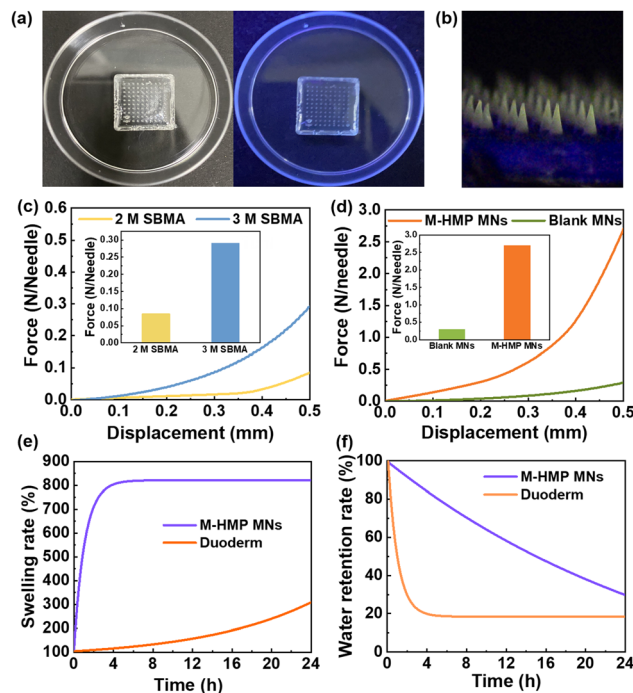


**Fig. 3** (a) Images of Blank MNs under natural light (left) and UV irradiation (right). (b) Images of ZnO-loaded tips under UV irradiation. (c) Displacement-force curve of the MNs made by different SBMA monomer concentrations. (d) Displacement-force curve of the blank MNs and M-HMP MNs. (e) Swelling rate of the M-HMP MNs substrates and Duoderm in AWE. (f) Water retention rate of the M-HMP MNs substrates and Duoderm.

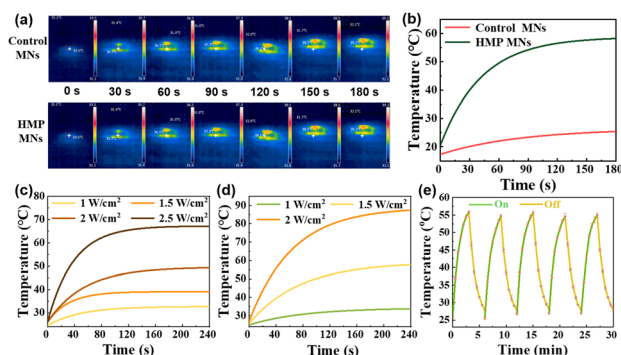


**Fig. 4** Photothermal properties of microneedles. (a) Thermal images of the MNs loaded with  $1 \text{ mg mL}^{-1}$  HMPs and without HMPs under irradiation. (b) Photothermal responsive profiles of the HMP MNs and blank MNs. Photothermal properties under different near-infrared light intensities of the MNs loaded: (c)  $0.5 \text{ mg mL}^{-1}$  and (d)  $1 \text{ mg mL}^{-1}$  HMPs. (e) Time-temperature curve of the MNs loaded with  $1 \text{ mg mL}^{-1}$  HMPs under the repeated on-off mode of irradiation.

the microneedles had good toughness and compression resistance properties. When the SBMA monomer concentration was raised to 4 M, the pre-polymerization solution became very viscous and difficult to add to the mold to form the microneedle tips. Thus, SBMA of 3 M was chosen to conduct the following experiments.

To be used as a wound dressing, the microneedle substrates should have a certain swelling rate and water retention rate so that they can absorb the wound exudate and keep moist, which can lead to fast wound recovery. So, the swelling rate and water retention rate of the zwitterionic microneedles were investigated using commercial wounding dressings as control. Fig. 3e shows that the swelling ratio of the M-HMP MNs could reach 800%. The extremely high swelling rate indicates that the microneedle substrates could quickly absorb the wound exudate, which is beneficial to wound healing. From Fig. 3f, it can be seen that the microneedles could still retain more than 85% of water at 4 h. In the meantime, the commercial wound dressing lost most of the water within 4 h, so it could not keep the wound moist. According to the reports,<sup>31</sup> the swelling rate and water retention rate of the microneedle substrates have met the requirement of wound dressings, which is very beneficial for wound healing.

The photothermal effect plays an important role in killing bacteria while promoting wound recovery. Therefore, to confirm the effect of the HMPs concentration and the power of NIR light on the photothermal effect of microneedles, the temperature profiles of HMPs at 0.5 mg mL<sup>-1</sup> and 1 mg mL<sup>-1</sup> were studied under irradiation of different light power, respectively. It can be seen that the temperature can reach 50 °C within 3 min at a concentration of 0.5 mg mL<sup>-1</sup> at a power of 2 W cm<sup>-2</sup> and 1 mg mL<sup>-1</sup> at a power of 1.5 W cm<sup>-2</sup> (Fig. 4c and d). Considering that too much power may cause skin damage, the HMPs concentration of 1 mg mL<sup>-1</sup> and the NIR light power of 1.5 W cm<sup>-2</sup> were chosen to prepare microneedles in this work.

Furthermore, to confirm the stability and repeatability of the photothermal conversion capacity of the M-HMPs MNs, the temperature cycles of the M-HMPs MNs were recorded by controlling the NIR light repeatedly on and off. It was shown that the temperature trends of the M-HMPs MNs were almost the same through 5 cycles, indicating that the M-HMPs MNs have a stable and repeatable photothermal effect (Fig. 4e). The high and sustainable photothermal conversion capacity shown by HMPs makes them an ideal material for achieving photothermal therapy.

Asiaticoside and ZnO NPs have been shown to kill Gram-negative bacteria and Gram-positive bacteria and fungi.<sup>23</sup> The antibacterial activity is due to the ring-breaking effect of cumene glycosides on bacterial biofilms and the release of Zn<sup>2+</sup> by ZnO NPs in the acidic environment under bacterial infection, which destroys the bacterial structure. When the M-HMP MNs are inserted into skins, the tips of the microneedles will be degraded and the asiaticoside and ZnO NPs are released simultaneously in the deep wound to perform their anti-bacterial function. To investigate the anti-bacterial function of the microneedles, different microneedle samples were placed into the individual bacterial solutions of *E. coli* and *S. aureus* for co-cultivation, and then the bacterial solutions were removed and applied on agar plates for the plate counting method.

As shown in Fig. 5a, the bacteria were significantly reduced in the HMP MNs + NIR, M MNs, and M-HMP MNs + NIR

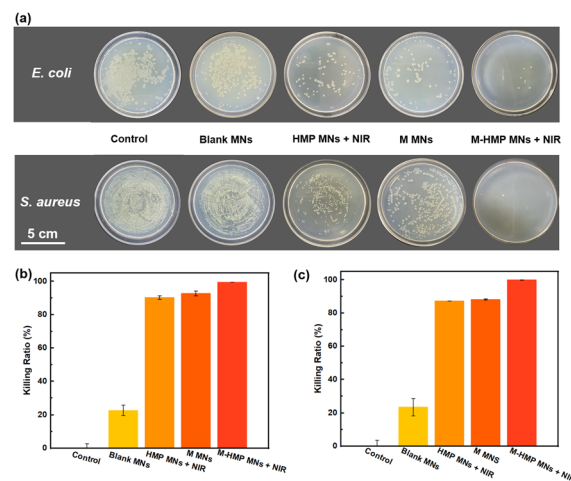
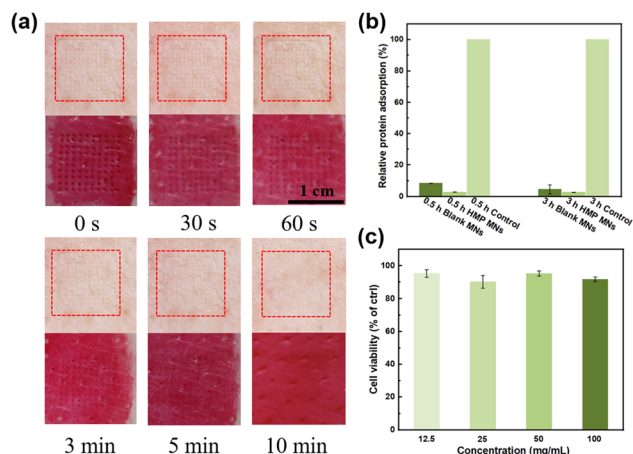


Fig. 5 *In vitro* antibacterial properties of microneedles. (a) Representative image formed by different MNs samples without or with NIR irradiation (808 nm, 1.5 W cm<sup>-2</sup>). The bacteria-killing efficiency against. (b) *E. coli* and (c) *S. aureus* ( $n = 5$ ).

groups compared with the control group. Among those, the M-HMP MNs + NIR group showed the most obvious inhibition effect on bacteria, while the blank MNs had almost no antibacterial effect. In detail, the mortality rates of both *E. coli* and *S. aureus* in the HMP MNs + NIR, M MNs group were higher than 80%, and the M-HMP MNs + NIR group had the best effect, which was close to 100%. These results indicated that both the photothermal effect and drugs loaded in the tips had contributed to the inhibition effect on bacteria. Moreover, by the combination of the two methods together, the anti-bacterial effect was achieved most.

Since microneedle patches require direct contact with the wound site, the biocompatibility of the M-HMP MNs must be investigated. First, M-HMP MNs were placed on treated pig skin and subjected to thumb pressure for 10 s. After removal, no visible skin damage was found at the microneedle pressed site, and the micropores left by the microneedles gradually disappeared over 5 min and completely disappeared after 10 min (Fig. 6a). The rapid resealing of the microchannels left by the microneedles prevents the entry of bacteria or toxic substances, thus reducing the risk of infection. HMP MNs have excellent anti-adhesive properties against nonspecific proteins (Fig. 6b), which can make it difficult for bacteria to adhere to the MNs, thus improving the antibacterial performance of MNs. Subsequently, mouse fibroblasts (L929 cells) were co-cultured with leachate of HMP MNs for one day, and the corresponding cell viability was tested to evaluate the *in vitro* cytotoxicity of M-HMP MNs. As shown in Fig. 6c, after one day of co-culture, the cell viabilities under all concentrations were above 90%. According to ISO 10993-5-2009, M-HMP MNs can be considered non-cytotoxic with cell viability, which is more than 80%, proving the good biocompatibility of microneedles.

Then, to verify the effect of the microneedles on chronic infected wounds, the infected wound model is artificially established on diabetic rats. The rats were in hyperglycemia



**Fig. 6** *In vitro* biocompatibility of microneedles. (a) Disappearance process of microneedle imprint on pig skin. (b) The relative HRP-conjugated IgG adsorption on the blank MNs and HMP MNs. (c) Viability of the L929 cell after incubation with the leachate solution of HMP MNs at different concentrations for 1 day.

during the entire treatment process (Table S1†). As shown in Fig. 7a, after the diabetic infected wound model was established, the rats were treated differently, as described in the Experimental section. To assess the treatment outcome of each group, photographs were taken after 0, 1, 3, 5, 7 and 10 d of treatment for detailed analysis (Fig. 7b). From Fig. 7b and d, the diabetic wound area gradually decreased over time in all groups, but at different rates. More specifically, compared with the control group, both the HMP MNs + NIR group and the M MNs group had faster-wound healing. The result proves that the photothermal effect and the loaded asiaticoside and ZnO NPs can promote wound healing. However, compared with the M-HMP MNs + NIR group, their healing effect was not as good. Statistical analysis of the data showed that the wound

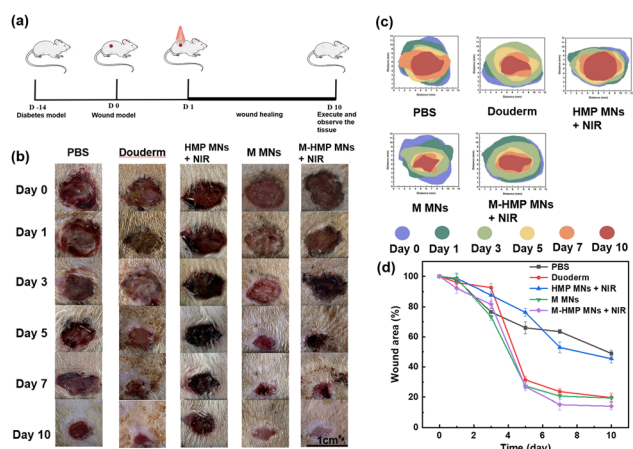


**Fig. 7** (a) Design of a model of skin defect wound in diabetes rats infected with *S. aureus*. (b) Representative images of the wounds from day 0 to day 10 with different treatments. (c) Simulation of changes in wound morphology within 10 days. (d) Quantitative analysis of the wound area at day 10 ( $n = 4$ ).

healing effect in the M-HMP MNs + NIR group was significantly better than that in other groups, with 84% of wounds healing and new skin growth after 10 days of treatment (Fig. 7d). All of the results suggest that the combination of asiaticoside and ZnO NPs and photothermal therapy exhibits a synergetic effect on infected wound healing in diabetics.

In the final stage of wound healing, skin composition remodeling is a key indicator of wound healing, which can be assessed by the thickness of granulation tissue at the wound site and the amount of collagen deposition. The rats were executed on day 10, and the wound site tissues were collected and stained with H&E (Fig. 8). The granulation tissues were red in color and new tissues, consisting of fibroblasts, inflammatory cells, and new blood vessels, appeared during the wound-healing phase. According to the tissue staining results, each group's thickness was quantified. The granulation tissue of the M-HMP MNs + NIR group was the thickest. Its thickness was 348.1 mm more than that of the control group (760 mm in the M-HMP MNs + NIR group, 411.9 mm in the control group), and was also significantly higher than that of the Douderm group (430 mm) and the HMP MNs + NIR group (563 mm). Through the macroscopic analysis of the wound area and granulation tissue, it was found that the combination of medicine and photothermal therapy had the best effect.

Collagen deposition is also commonly used to assess wound healing. In the results of the MTS (Fig. 9), collagen

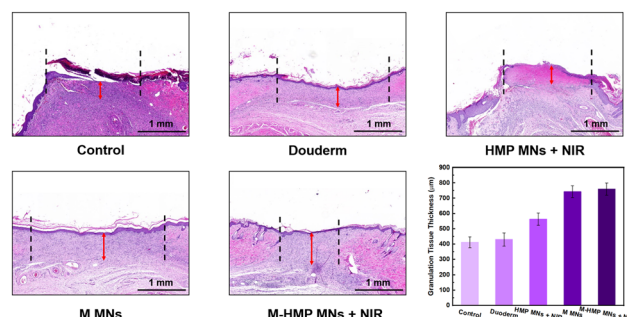


**Fig. 8** H&E staining of healed skin in different groups and quantitative analysis of the epithelial tissue thickness. Data are shown as mean  $\pm$  SD ( $n = 3$ ).

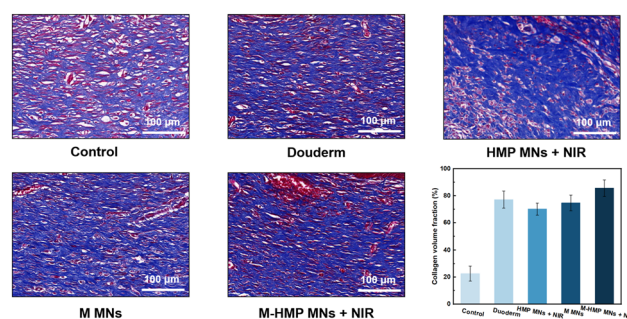


**Fig. 9** Collagen deposition was analyzed by Masson's trichrome staining after 9 days. Data are shown as mean  $\pm$  SD ( $n = 3$ ).



fibers are blue and muscle fibers are red. Compared with the control group, the content of collagen fiber in the M MNs group and the M-HMP MNs group is higher, and the tissue is more compact. In addition, in the M-HMP MNs group, a large area of new collagen stained with dark blue was directionally arranged in the new epithelial tissue, indicating that the amount of collagen deposition was increased and tissue remodeling was improved.

## Conclusions

In this work, a new kind of multifunctional zwitterionic micro-needle dressing was developed to achieve wound healing and tissue regeneration in chronically infected diabetic wounds. The unique structure of the microneedle can penetrate the skin and deliver drugs to the deep wound. With the degradation of the tips, ZnO and asiaticoside were released for wound sterilization and tissue reconstruction. The antifouling substrates containing HMPs combined with the near infrared kill bacteria and accelerate wound healing. Results proved that the M-HMP MNs exhibited excellent antibacterial effect *in vivo* and *in vitro*, and it could promote granulation and collagen deposition of chronic wounds to accelerate their healing. These characteristics make M-HMP MNs a promising candidate for clinical wound healing.

## Ethical statement

All animal procedures were performed in accordance with the Guidelines for Care and Use of Laboratory Animals of “Zhejiang Center of Laboratory Animals”, and approved by the Animal Ethics Committee of “Zhejiang Center of Laboratory Animals” with the ethical code of ZJCLA-IACUC-20020092.

## Conflicts of interest

There are no conflicts of interest to declare.

## Acknowledgements

This work was funded by the National Natural Science Foundation of China [Grants 52073256 and 21404091], and the Natural Science Foundation of Zhejiang Province [LBY21E030001]. This research was also supported by the Institute for Frontiers and Interdisciplinary Sciences, Zhejiang University of Technology [2022JCY01].

## References

- 1 V. Falanga, *Lancet*, 2005, **366**, 1736–1743.
- 2 R. Jamaledin, C. K. Y. Yiu, E. N. Zare, L. Niu, R. Vecchione, G. Chen, Z. Gu, F. R. Tay and P. Makvandi, *Adv. Mater.*, 2020, **32**, 2002129.
- 3 F. Rademacher, M. Simanski, R. Gläser and J. Harder, *Exp. Dermatol.*, 2018, **27**, 489–494.
- 4 J. Xiao, S. Chen, J. Yi, H. F. Zhang and G. A. Ameer, *Adv. Funct. Mater.*, 2017, **27**, 1604872.
- 5 A. J. Singer and R. A. F. Clark, *N. Engl. J. Med.*, 1999, **341**, 738–746.
- 6 A. J. Guillot, A. S. Cordeiro, R. F. Donnelly, M. C. Montesinos, T. M. Garrigues and A. Melero, *Pharmaceutics*, 2020, **12**, 569.
- 7 W. Y. Jeong, M. Kwon, H. E. Choi and K. S. Kim, *Biomater. Res.*, 2021, **25**, 24.
- 8 Y. Hao, W. Li, X. Zhou, F. Yang and Z. Qian, *J. Biomed. Nanotechnol.*, 2017, **13**, 1581–1597.
- 9 K. Ahmed Saeed AL-Japairai, S. Mahmood, S. Hamed Almurisi, J. Reddy Venugopal, A. Rebhi Hilles, M. Azmana and S. Raman, *Int. J. Pharm.*, 2020, **587**, 119673.
- 10 L. Zhang, R. Guo, S. Wang, X. Yang, G. Ling and P. Zhang, *Int. J. Pharm.*, 2021, **604**, 120749.
- 11 R. D. Koyani, *J. Drug Delivery Sci. Technol.*, 2020, **60**, 102071.
- 12 J. Wang, L. Wang, C. Wu, X. Pei, Y. Cong, R. Zhang and J. Fu, *ACS Appl. Mater. Interfaces*, 2020, **12**, 46816–46826.
- 13 Q. Li, C. Wen, J. Yang, X. Zhou, Y. Zhu, J. Zheng, G. Cheng, J. Bai, T. Xu, J. Ji, S. Jiang, L. Zhang and P. Zhang, *Chem. Rev.*, 2022, **122**(23), 17073–17154.
- 14 C. Pouget, C. Dunyach-Remy, A. Pantel, S. Schuldiner, A. Sotto and J.-P. Lavigne, *Microorganisms*, 2020, **8**, 1580.
- 15 Y. Hu, H. Li, X. Lv, Y. Xu, Y. Xie, L. Yuwen, Y. Song, S. Li, J. Shao and D. Yang, *Nanoscale*, 2022, **14**, 12967–12983.
- 16 X. Li, J. F. Lovell, J. Yoon and X. Chen, *Nat. Rev. Clin. Oncol.*, 2020, **17**, 657–674.
- 17 X. Zhao, Y. Liang, Y. Huang, J. He, Y. Han and B. Guo, *Adv. Funct. Mater.*, 2020, **30**, 1910748.
- 18 D.-W. Zheng, S. Hong, L. Xu, C.-X. Li, K. Li, S.-X. Cheng and X.-Z. Zhang, *Adv. Mater.*, 2018, **30**, 1800836.
- 19 X. Zhang, G. Chen, Y. Liu, L. Sun, L. Sun and Y. Zhao, *ACS Nano*, 2020, **14**, 5901–5908.
- 20 M. Godoy-Gallardo, U. Eckhard, L. M. Delgado, Y. J. D. de Roo Puente, M. Hoyos-Nogués, F. J. Gil and R. A. Perez, *Bioact. Mater.*, 2021, **6**, 4470–4490.
- 21 X. Xie, X. Jin, B. He, Y. Zou, J. Yang, C. Liu, X. Kong, W. Liu and W. Wang, *Appl. Mater. Today*, 2022, **27**, 101477.
- 22 M. S. Saddik, M. M. A. Elsayed, M. A. El-Mokhtar, H. Sedky, J. A. Abdel-Aleem, A. M. Abu-Dief, M. F. Al-Hakkani, H. L. Hussein, S. A. Al-Shelkamy, F. Y. Meligy, A. Khames and H. A. Abou-Taleb, *Pharmaceutics*, 2022, **14**, 111.
- 23 S. V. Gudkov, D. E. Burmistrov, D. A. Serov, M. B. Rebezov, A. A. Semenova and A. B. Lisitsyn, *Front. Phys.*, 2021, **9**, 641481.
- 24 S. Saidin, M. A. Jumat, N. A. A. M. Amin and A. S. S. Al-Hammadi, *Mater. Sci. Eng., C*, 2021, **118**, 111382.
- 25 D. Lahiri, M. Nag, H. I. Sheikh, T. Sarkar, H. A. Edinur, S. Pati and R. R. Ray, *Front. Microbiol.*, 2021, **12**, 636588.
- 26 S.-E. Jin and H.-E. Jin, *Nanomaterials*, 2021, **11**, 263.
- 27 X. Y. He, A. Sun, T. Li, Y. J. Qian, H. Qian, Y. F. Ling, L. H. Zhang, Q. Y. Liu, T. Peng and Z. Qian, *Carbohydr. Polym.*, 2020, **247**, 116692.



- 28 J. Zhang, L. Chen, J. Chen, D. Wu and J. Feng, *J. Appl. Polym. Sci.*, 2018, **135**, 45831.
- 29 Y. Zhu, J. Zhang, J. Song, J. Yang, Z. Du, W. Zhao, H. Guo, C. Wen, Q. Li, X. Sui and L. Zhang, *Adv. Funct. Mater.*, 2020, **30**, 1905493.
- 30 Y. Li, X. Hu, Z. Dong, Y. Chen, W. Zhao, Y. Wang, L. Zhang, M. Chen, C. Wu and Q. Wang, *Eur. J. Pharm. Sci.*, 2020, **151**, 105361.
- 31 S. Jacob, A. B. Nair, J. Shah, N. Sreeharsha, S. Gupta and P. Shinu, *Pharmaceutics*, 2021, **13**, 357.